

Manuscript Number: COMMAT-D-16-01815R1

Title: Identification of key liquid metal flow features in the physical conditioning of molten aluminium alloy with high shear processing.

Article Type: Full Length Article

Section/Category: Large Scale Systems

Keywords: rotor-stator mixer; high shear processing; computer simulation; shear rate; flow rate; aluminium alloy purification

Corresponding Author: Professor David J, Browne, D.Phil.

Corresponding Author's Institution: University College Dublin

First Author: Mingming Tong, PhD

Order of Authors: Mingming Tong, PhD; Jayesh B Patel, PhD; Ian Stone, PhD; Zhongyun Fan, PhD; David Browne, PhD

Abstract: Although treating molten alloy with high shear processing (HSP) can dramatically refine the microstructure of solidified aluminium alloys, it was also recently employed as part of an effective route to purification of contaminated aluminium alloy scrap. The key mechanisms of HSP include the dispersion of large aluminium oxide films and clusters into very fine oxide particles by the high shear rate, and the redistribution of bulk melt by the agitation. These fine oxides act as nucleation sites for iron-based intermetallic phases, the formation of which is a pre-cursor to purification of the alloy. Macroscopic flow features of HSP, such as flow rate and shear rate, influence its performance significantly. Simulation based on Computational Fluid Dynamics was used to predict key features of fluid flow during HSP in a static direct chill (DC) caster. It was found that the distribution of shear rate and mass flow rate is highly nonuniform in the caster, and only in the close vicinity of the mixing head is there a relatively high level of shear rate and effective melt agitation. Therefore, effective dispersion of oxide films and clusters, and resulting significant nucleation of the intermetallics and/or primary aluminium phase, can only occur near the mixing head, and not throughout the whole crucible. Confidence in the model validity was built, by comparison with post-solidification microstructures in a previous experiment with similar process parameters and geometry.



UCD School of Mechanical and
Materials Engineering

Scoil na hInnealtóireachta
Meicniúla agus Ábhar UCD

University College Dublin,
Belfield, Dublin 4, Ireland

An Coláiste Ollscoile Baile Átha Cliath,
Belfield, Baile Átha Cliath 4, Éire

T +353 1 716 1884/1787/1757
F +353 1 283 0534

mme@ucd.ie
www.ucd.ie/eacollege/mme/

Prof. Jeffrey Hoyt
Associate Editor
Computational Materials Science

27 January 2017

Dear Professor Hoyt,

I refer to the revision of our manuscript *Identification of key liquid metal flow features in the physical conditioning of molten aluminium alloy with high shear processing*. As highlighted in the manuscript by using red font, we have carefully revised the document according to the advice of the Reviewer. We believe we have addressed the Reviewer's concerns. As a result, we hope the improved contribution can be accepted for publication in Computational Materials Science.

The specific replies to all the Reviewer's comments are itemised separately in our document "Response to Reviewers". I thank you very much for coordinating the review of this paper, and look forward to hearing from you on this matter.

Yours sincerely,

A handwritten signature in black ink, appearing to read 'David Browne', with a long horizontal flourish extending to the right.

David J. Browne, D.Phil.

Associate Professor of Materials Science & Engineering

*Vice-Principal for Research, Innovation & Impact
College of Engineering & Architecture*

Direct tel: +353 1 716 1901; mobile: +353 86 837 6647; email: david.browne@ucd.ie

Response to Reviewers

Manuscript COMMAT-D-16-10815

Identification of key liquid metal flow features in the physical conditioning of molten aluminium alloy with high shear processing

All the commentary of the Reviewer has been reprinted below, split into a number of Comments. We hereby provide a Reply to each such Comment.

Comment A:

The conditioning of molten alloys, using severe shearing to achieve grain refinement, is well documented in the literature and the research group of Prof. Fan, one of the authors, has contributed to this research. The concurrent effects of shearing on either the heterogeneous nucleation of solid phase from fragmented oxides or the purification of alloys melts, e.g., by precipitation of heavy polluting Fe phases in aluminum alloys, are recent observations and thus requires more investigation.

The manuscript is in line with these new research issues, therefore very welcome.

Reply A:

The authors welcome these introductory comments by the Reviewer.

Comment B:

However, despite the attractive Introduction, the presented CFD model and its results cannot provide a sound scientific methodology to explain the metallurgical effects induced by severe shearing of aluminum melt flow. Moreover, the final experimental validation, discussed in the last section, has to be considered as a pure speculation rather than an expected genuine comparison between experiments and model predictions. The authors carelessly attempt to correlate observed grain size with predicted shear rate effects ignoring completely any cooling effect.

Reply B:

We recognise that the current CFD model cannot predict grain size evolution in the solidified ingot. We note that high shear rates cause oxide fragmentation, and that although the link between this and nucleation of intermetallics or primary Al is not simulated in our work, we believe that Figs. 14 and 15 (of revised MS) provide confidence in the accuracy of the current simulation. We have cited another report, by separate authors [10], that independently shows that shearing of liquid aluminium alloys, prior to solidification, reduces as-cast grain size. We have modified the text (last sentence of Abstract, last sentence of Section 1, and new paragraph 2 in Section 4 - Discussion) also to downgrade any claims of direct model validation. We have also noted (also the new paragraph 2 in Section 4) that we need to model heat transfer and solidification to provide direct validation from these experiments.

Comment C:

Note that, the rotor-stator unit itself, due to such high speed rotation may induce in the melt a convection cooling which is neglected.

Reply C:

The research that is presented in this work is trying to identify the key features of liquid metal flow in HSP. The problem of heat transfer is not within the scope of this manuscript.

Comment D:

In order to promote a genuine growth of science, any experimentally validated model has to show one-to-one comparisons between observed and predicted quantities, say, predicted grain size and observed grain size, observed solid fraction and predicted solid fraction and so on. By reading the article one wonders: how a pure CFD analysis, which does neither accounts for neither thermal field nor solidification phenomena, can be capable of providing useful and unambiguous information on solidification structure and particularly grain size?

Reply D:

This comment is an expansion of Comment B above, and so our Reply B is also relevant here. The primary goal of this research is the purification of Al alloys by high shear to cause

fragmentation of oxides which will then act as nucleating agents for Fe-bearing intermetallics. These intermetallics can then be removed by sedimentation. This is explained in the Abstract, but now also reinforced by additional text in the Introduction. That is why the numerical modelling of the process is so important. In the alloy purification, the shear rate and melt re-distribution is critical. However if the fine oxide/intermetallic particles are not removed from the melt, then they can act as physical grain-refiners [10]. This is the case in the experiment of Ref. [23]. We have shown that the areas of the crucible where the shear rate has been highest have shown the finest as-cast grain size. The validation is not direct, and we now say (see modified Abstract) that this is just a confidence-building measure. We believe it to be logically sound, given previous studies of the effects of such shearing. The Reviewer has made us think harder about this issue, and we have modified our position to be more defensible. In this way the Reviewer has helped to improve the manuscript, for which we are grateful.

Comment E:

If the final target of the work focuses on metallurgical aspects, and the authors decide to neglect any appropriate modeling, the reader expects that at least a proved scientific methodology is proposed to bridge the gap between CFD analysis and metallurgical phenomena. Instead, the authors attempt this by an unproven rationale. Thus, in the absence of a suitable thermal model (possibly also a solidification model) or such a scientific proof between CFD results and experimental metallurgical results any conclusion drawn by the authors has to be considered as speculative which cannot be accepted.

Reply E:

We agree with this point, which is also relevant to Comments (and Replies) B and D above. This manuscript is about a CFD model which has been carefully set up to simulate the experiment from the literature, and be relevant to alloy purification/recycling. The grain sizes in the experiments are no longer being claimed as validation of the model, merely as supporting and relevant data – necessary but not sufficient. We have also developed (but in 2D only so far) a model of oxide fragmentation in the process [12] and have started work on correlation of intermetallic nucleation dynamics to the resulting set of particles, with their own size (and therefore nucleation activation undercooling) distributions. Experimental validation of such predictions will be extremely difficult.

Comment F:

Nevertheless, as the CFD model itself has its own merits, if it was used to assess the design of the rotor-stator mixer unit, from a pure fluid dynamic point of view, the appropriate boundary conditions were specified and the CFD model be validated against appropriate flow field quantities, it can be worth of publication. Alternatively, if the temperature field could be coupled in the CFD model and solved simultaneously, the experimental validation against temperature probes and some metallurgical features could be fair.

Reply F:

The CFD aspects of the model, and boundary conditions, have been explained in more detail (Section 2) in the revised text , and further details of the rotor-stator mixer have been included (more detailed labelling in Fig. 1 and a new solid model of the mixer – Fig. 2).

With regard to model validation, the research we present is trying to identify the key features of liquid metal flow in the physical conditioning of molten aluminium alloy with high shear processing. To date, it has been very difficult (or impractical) to experimentally measure the flow features inside an opaque liquid metal. Because the molten metal is non-transparent and at high temperature, it is infeasible or dangerous to place experimental measurement equipment very close to the liquid that is being treated by HSP when operating the mixer. After doing an exhaustive literature review, we found that there is no related experimental work published. Therefore, it is impractical to do direct one-to-one comparisons between the observed and predicted quantities, with regard to the fluid flow inside an opaque liquid metal. Although the experimental validation we presented is indirect, the authors did careful and comprehensive analysis and comparison of related data and the results (figures and text of Section 3.5) positively supported the computational work in a reasonable way.

Comment G:

A minor criticism, but also important, concerns the excessive self-citation: almost half of the 27 references come from Dr. Fan!! This number should be decreased markedly.

Reply G:

First of all, we agree with the referee that the citation should cover as wide spectrum as possible of the state-of-the-art research in related field of research. However, after the

exhaustive literature review, we realized that most of the publications in connection with the physical conditioning of molten metal using the high shear processing for the purpose of either microstructure refinement or material purification come from the research centre of Prof. Fan. This research centre turns out to be the most active research team that has been recently conducting related research. Citing those references of Prof. Fan's team in this paper is the reflection of the state-of-the-art research of this topic.

We have also added another supporting publication by Haghayeghi and Nastac, one of 8 more references added following the review – none by Fan. So that dilutes the proportion of cited references that are from Fan's group.

Comment H:

Two additional scientific comments follow below. The first, relates with the observations that fragmentation of oxides by severe flow shearing may be the driving force for nucleation of the new solid phase. In contrast with this the CFD results show that the shear rate decreases by various order of magnitude when passing from inside the stirring unit to outside the DC caster. Indeed, experiments show that even very low flow shearing suffices to produce quite different grain size and morphologies in the casting away from the unit. This, in turn, would suggest that: a) provided that flow agitation is in general beneficial for grain size refinement, such so high speed-rotor stirring unit is not really necessary to homogenize castings; b) by contrast, oxide fragmentation would not, in fact, be the leading influencing factor for homogenization, since these would require extremely high shear rates.

Reply H:

Neither this paper nor the overall research activity of the authors is targeting the homogenization of castings. We are researching HSP, conducted for the purpose of molten metal purification, rather than homogenization. This is highlighted in the second, third and the last paragraph of the revised manuscript. We investigate here the key features of liquid metal flow, the target of which is to fragment the oxides by the high shear. Whether such high shear rates are really necessary for grain refinement is an open question, but ref. [23] shows that they are sufficient.

Comment I:

The second comment pertains to the real benefits imparted by the patented stirring unit itself. This unit utilizes very high rotor speed energy to shear the molten metal sucked inside with low efficacy. Then the designed rows of holes in the outer stator readily destroy this acquired energy by the fluid. Mechanically speaking, this unit resembles more an energy dissipator rather than a mixer. It is a mechanical expedient which consumes high mechanical energy to produce minor metallurgical results. Thus, based on shown results, the effects induced by the said stirring unit might be of scientific interest but its effectiveness and efficiency in industrial casting manufacturing, remains to be proved. Based on this latter point, the Introduction section should be arranged accordingly to avoid misleading science and technology.

Reply I:

We do not believe that we have made any un-substantiated claims in the Introduction – all points are backed up with appropriate citations in the international literature. Some of that literature does not use the same mixer as is the subject of the current contribution. We also do not claim to have studied its efficiency, merely its effectiveness. Indeed a re-design would be required to make the device suitable for industrial processing of metals – as attested to by the limitations highlighted by our simulations.

We call the patented high shear unit a mixer because this type of facility is commonly or commercially known as a mixer. In our work, this high shear unit is not used for the purpose of mixing at all and the research is not about casting manufacture. By significantly dissipating energy, as correctly noted by the Reviewer, this high shear unit can very effectively disperse the oxide clusters, because the characteristic shear rate (responsible for the fragmentation of oxide clusters) is directly and positively dependent on the turbulence energy dissipation rate (Ref [12] of this paper) of the turbulent flow of the liquid metal.

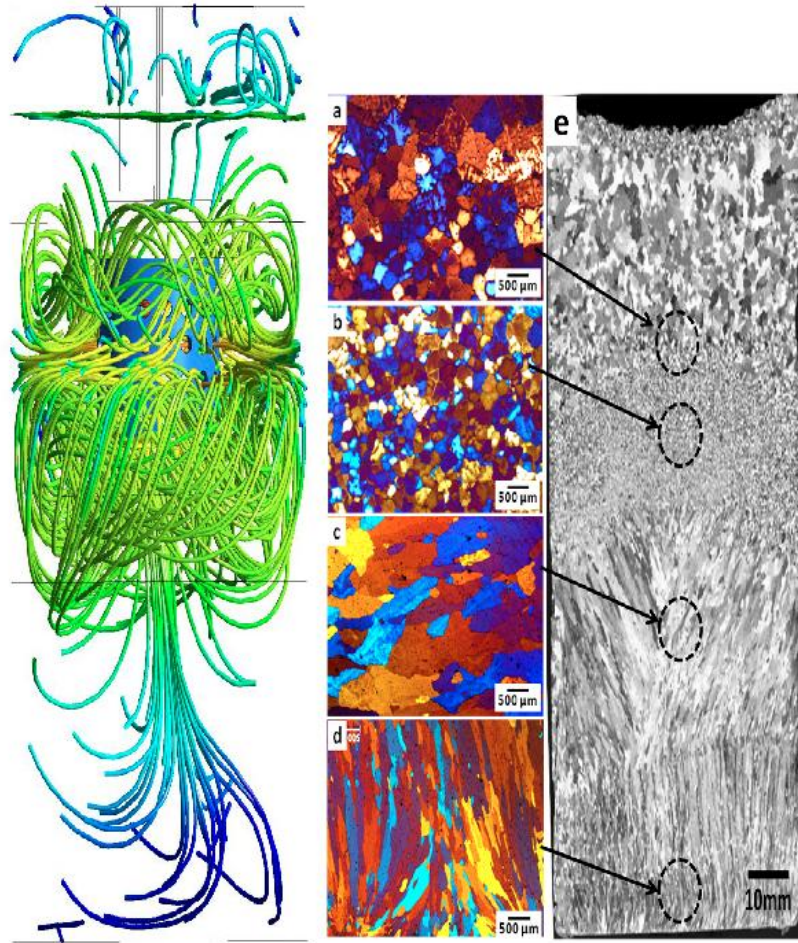
Comment J:

In conclusion, the paper is accepted provided that the suggested major revisions are accomplished.

Reply J:

We believe that we have revised the paper to make most of the suggested improvements, and taken account of them all in the new version.

Graphical Abstract



Highlights

- Shear rate and mass flow rate are computationally predicted with CFD for HSP of liquid metal
- The proposed application is purifying liquid aluminium alloy to aid recycling
- Flow features of melt are highly non-uniform during HSP
- High level of shear rate and mass flow rate only exist in the close vicinity of the mixing head
- Experimental measurements positively support our simulation results.

1 Identification of key liquid metal flow features in the physical conditioning of molten
2 aluminium alloy with high shear processing

3 Mingming Tong^{1,2}, Jayesh B. Patel³, Ian Stone³, Zhongyun Fan³, David J. Browne^{1*}

4
5
6 1. School of Mechanical and Materials Engineering, University College Dublin, Ireland

7 2. Present address: Mechanical Engineering, NUI Galway, Ireland

8 3. BCAST, Brunel University, UK
9

10
11
12 * Corresponding author – david.browne@ucd.ie
13
14

15
16 Abstract
17

18 Although treating molten alloy with high shear processing (HSP) can dramatically refine the
19 microstructure of solidified aluminium alloys, it was also recently employed as part of an
20 effective route to purification of contaminated aluminium alloy scrap. The key mechanisms
21 of HSP include the dispersion of large aluminium oxide films and clusters into very fine
22 oxide particles by the high shear rate, and the redistribution of bulk melt by the agitation.
23 These fine oxides act as nucleation sites for iron-based intermetallic phases, the formation of
24 which is a pre-cursor to purification of the alloy. Macroscopic flow features of HSP, such as
25 flow rate and shear rate, influence its performance significantly. Simulation based on
26 Computational Fluid Dynamics was used to predict key features of fluid flow during HSP in
27 a static direct chill (DC) caster. It was found that the distribution of shear rate and mass flow
28 rate is highly nonuniform in the caster, and only in the close vicinity of the mixing head is
29 there a relatively high level of shear rate and effective melt agitation. Therefore, effective
30 dispersion of oxide films and clusters, and resulting significant nucleation of the
31 intermetallics and/or primary aluminium phase, can only occur near the mixing head, and not
32 throughout the whole crucible. Confidence in the model validity was built, by comparison
33 with post-solidification microstructures in a previous experiment with similar process
34 parameters and geometry.
35
36
37
38
39
40
41
42
43
44
45
46
47
48
49
50
51
52

53 Keywords: rotor-stator mixer, high shear processing, computer simulation, shear rate, flow
54 rate, aluminium alloy
55
56
57
58
59
60
61
62
63
64
65

1. Introduction

1
2 Treating liquid metal with high shear processing (HSP) has been found to have significant
3 influence on the properties of solidified aluminium alloys and magnesium alloys. As
4 reviewed by Fan and co-workers [1,2], shearing the molten alloy in the liquid state using a
5 rotor-stator mixer can dramatically refine the microstructure of direct chill (DC) cast
6 aluminium alloys. Specifically, the HSP process can produce very fine equiaxed dendrites in
7 the cast alloy [3] without using grain refiners. The high shear rate generated by the closed
8 coupled rotor-stator mixer effectively fragments large aluminium oxide films and clusters
9 into fine individual particles [4]. In high grade aluminium alloys, in which the content of iron
10 and manganese is relatively low, the oxide particles were found to have very low lattice
11 misfit with the α -Al phase on close packed crystallographic planes [5]. On cooling liquid
12 aluminium alloys that have a relatively high level of iron (e.g. 1 wt% or higher), the iron-
13 bearing intermetallics normally precipitate before the appearance of α -Al phase [6]. The
14 lattice misfit between the aluminium oxide and iron bearing intermetallics was also found to
15 be very low [7]. Therefore, the fine oxide particles act as potent nucleation sites for both the
16 intermetallic and α -Al phases [8,9], during the solidification of aluminium alloys, and hence
17 refine the microstructure of corresponding cast samples. Haghayeghi and Nastac have also
18 reported [10] that shearing of a molten aluminium alloy prior to solidification resulted in a
19 finer equiaxed grain size.

20
21
22
23
24
25
26
27
28
29
30
31
32
33
34
35
36
37 Besides the influence on microstructure refinement, it has recently been realized that HSP has
38 great potential in purifying contaminated aluminium alloys. Iron is a very common and usually
39 detrimental impurity in recycled aluminium alloys. An excessive level of iron can dramatically
40 reduce the mechanical properties of the cast products. Due to the related thermodynamic features
41 of such alloys [6,8], iron-bearing intermetallics (e.g. α AlFeMnSi) can effectively collect the iron
42 component from molten scrap alloy while the primary α -Al solid solution phase is not yet formed
43 [11]. Because the solid intermetallics are denser than the rest of the molten alloy, they can be
44 separated from the bulk material by using a sedimentation technique, and hence the level of iron
45 in the treated material is decreased. Such physical conditioning of the molten alloy using HSP is
46 being used as the major technique in research on alloy purification, whereby the authors are
47 trying to manufacture high performance aluminium alloys by processing contaminated recycled
48 aluminium scrap.

1
2
3
4
5
6
7
8
9
10
11
12
13
14
15
16
17
18
19
20
21
22
23
24
25
26
27
28
29
30
31
32
33
34
35
36
37
38
39
40
41
42
43
44
45
46
47
48
49
50
51
52
53
54
55
56
57
58
59
60
61
62
63
64
65

With the purpose of purifying the contaminated material, the key factor of HSP is the shear of molten metal by the rotor-stator mixer. The nucleation of iron-bearing intermetallics or primary α -Al phase is only effective when there is large number of available potent nucleation sites present. As presented in previous work [12], the shear rate was found to have a dominant influence on the breakage of oxide clusters during HSP. In order to systematically understand the influence of HSP process parameters on the resultant size of oxides, the flow features of the liquid metal (including particularly the shear rate and flow rate of melt) during the HSP with rotor-stator mixer have to be characterised.

Although there are a variety of experimental methods that are capable of measuring the features of fluid flow, such as Laser Doppler Anemometry and Particle Image Velocimetry, they are very difficult to apply in the measurement of flow features inside an opaque liquid metal. Because the molten metal is non-transparent, at high temperature and maybe flammable (e.g. magnesium alloys), it is infeasible or dangerous to place such experimental measurement equipment very close to the liquid that is being treated by HSP when operating the mixer. Therefore, computer modelling and simulation provide a very good alternative to calculate the related key features of melt flow during HSP.

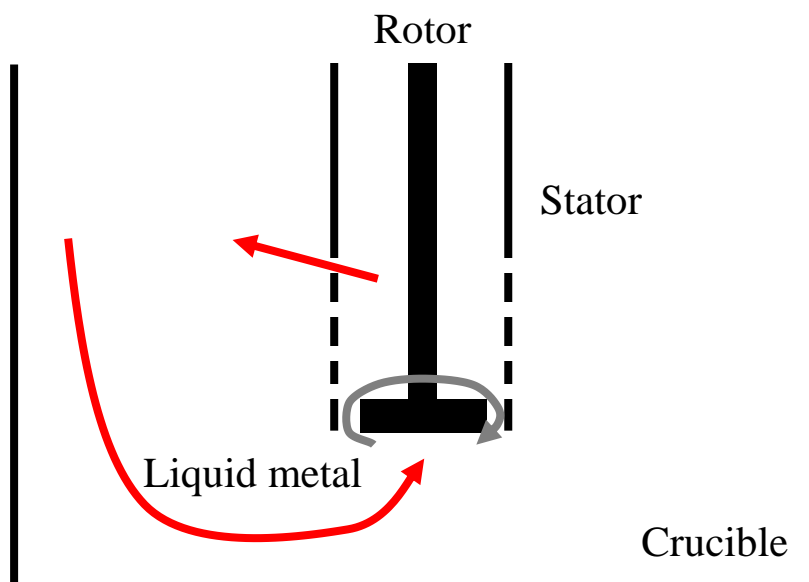
Using computational fluid dynamics (CFD), computer simulation has been extensively employed in the prediction of flow features of metal processing, including such as casting [13] and welding [14,15]. In comparison, CFD modelling of melt conditioning is relatively rare. The majority of this has been dedicated to the degassing processes taking place in the gas stirred ladle of liquid metals [16-18]. CFD modelling has been applied to precipitation processes occurring in a mechanically agitated tank [19], in which a standard combination of baffle and impeller is used to agitate the fluid. However, the rotor-stator mixer that is used in HSP is such a closely coupled device [1,20] that it is inherently different from such a baffle-impeller combination. The published CFD modelling that is most relevant to the HSP process of our interest is the work by Utomoa et al. [21, 22], in which a variety of flow features were analysed in the 3D CFD modelling of treating water with a rotor-stator mixer [21, 22]. However, respective results were only analysed along the radius of the mixer and there were no analyses of flow features through the depth of the tank. Moreover, the rotor-stator mixer that was employed in the research of [21,22] is a type of commercially available mixer with major applications in food, cosmetics, chemical and pharmaceutical industries. The novel rotor-stator mixer that is employed in the HSP of liquid metal [1,20] is a recently invented

1 device. Its design is very different from that of the conventional mixer (e.g. those used in
2 [21,22]). Taking the dramatic differences between the properties of liquid metal (e.g. liquid
3 aluminium alloy) and those of water into account (e.g. in terms Weber number and Prandtl
4 number), we have had to develop a new CFD model in order to understand and predict the
5 flow features of interest in the case of treating liquid metal with HSP.
6
7
8
9

10 In this paper, we firstly specify the configuration of the experimental device and
11 computational case study. Then we present the details of our computational model and
12 computer software. The key features of fluid flow simulations are analysed. Key
13 computational predictions are compared with available experimental results from an HSP-
14 treated solidified ingot, in order to **provide confidence in** the model.
15
16
17
18
19
20
21

22 2. Configuration of the case study and CFD model

23
24
25 The detailed configuration of treating liquid metal with HSP by using rotor-stator mixer can
26 be found in the Fig.1 of [23]. Figure 1a of the current paper schematically illustrates the
27 overall setup of HSP of liquid metal, and Fig.1b specifies some key dimensions of the mixing
28 head, **the 3D shape of which can be seen in Fig. 2**. In the crucible (or mould), the impeller
29 operates at relatively high speed. At the side of the stator near the mixing head, there are rows
30 of small holes, numbered as shown in Fig. 1b. At the bottom of the mixing head, there is a
31 relatively large opening. The liquid metal can flow in and out of the mixing head through
32 these holes and opening.
33
34
35
36
37
38
39
40
41
42
43
44
45



1
2
3
4
5
6
7
8
9
10
11
12
13
14
15
16
17
18
19
20
21
22
23
24
25
26
27
28
29
30
31
32
33
34
35
36
37
38
39
40
41
42
43
44
45
46
47
48
49
50
51
52
53
54
55
56
57
58
59
60
61
62
63
64
65

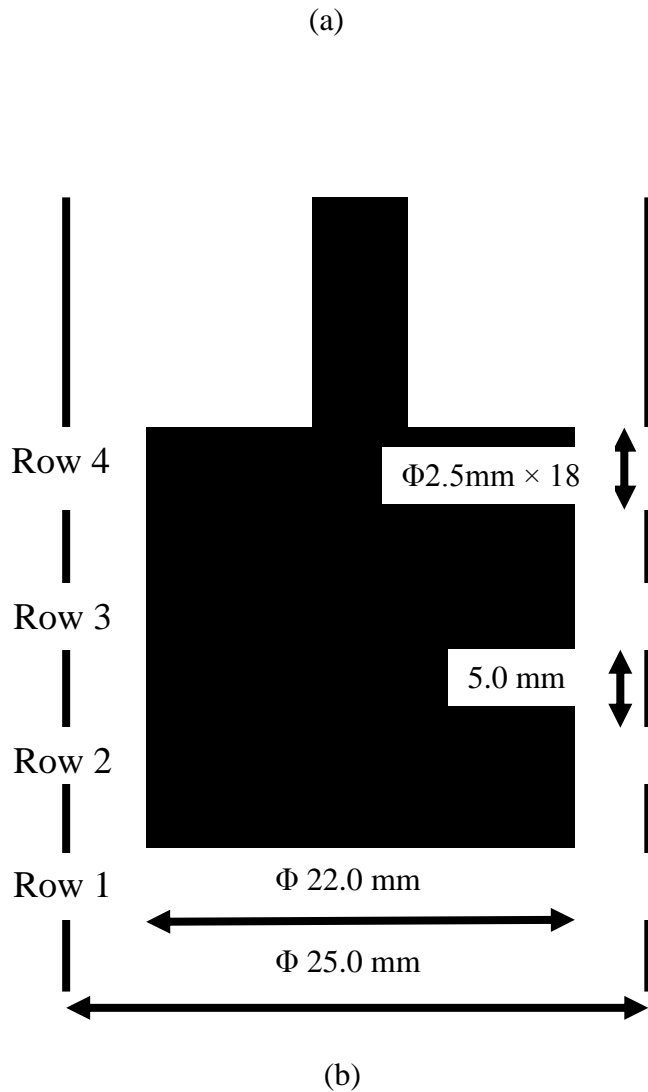


Fig.1. Configuration of HSP process including the (a) overall setup, and (b) key dimensions of the mixing head

The static DC caster is a cylindrical container of 60 mm in diameter. It is filled with liquid AA6060 aluminium alloy, to a depth of 120 mm. The rest of the caster contains air, above the liquid metal. The intent is to model the experiment carried out by Jones et al. [23], in which the mixer was removed from the superheated melt prior to alloy solidification. The mixer consists of a high speed spinning rotor and a stationary stator, which are coaxial and separated by a very small gap. The rotor consists of a long shaft with an impeller at its end, having four flat blades. The stator is a hollow tube, near the end of which is a series of circular holes in the wall. The geometry of the head of the mixer (i.e. the mixing head) can be seen in Fig.1. As stated, the specific 3D geometrical features of the mixing head are

1
2
3
4
5
6
7
8
9
10
11
12
13
14
15
16
17
18
19
20
21
22
23
24
25
26
27
28
29
30
31
32
33
34
35
36
37
38
39
40
41
42
43
44
45
46
47
48
49
50
51
52
53
54
55
56
57
58
59
60
61
62
63
64
65

illustrated in Fig.2. The outer and inner diameters of the stator are 25 mm and 22 mm, respectively, and the diameter of the impeller is 21.5 mm. The rotor-stator annular gap is therefore 0.25mm. There are 72 radial holes of 2.5 mm diameter in the stator, which are aligned along four rows or rings (of 18 equally spaced holes each). The impeller blades are 19 mm long. The mixer is placed inside the static DC caster at a depth of 70 mm relative to the bottom of the mixing head. The impeller speed is 4000 rpm.

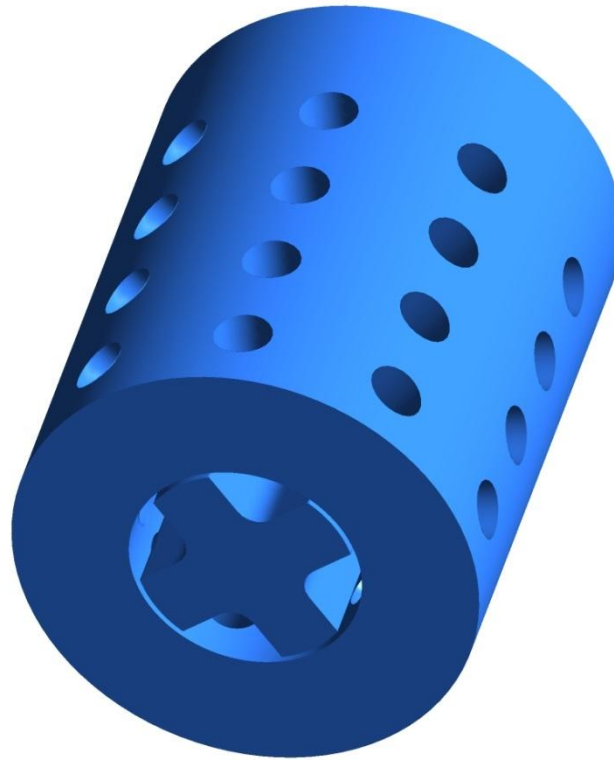


Fig.2. 3D geometrical features of the mixing head

The overall fluid flow problem is mathematically formulated with the conservation equations of mass and momentum, in 3D Cartesian coordinates:

$$\frac{\partial \rho}{\partial t} + \nabla \cdot (\rho \vec{V}) = 0, \tag{1}$$

$$\frac{\partial \rho \vec{V}}{\partial t} + \nabla \cdot (\rho \vec{V} \vec{V}) = -\nabla p + \nabla \cdot \bar{\bar{\tau}} + \vec{F}, \tag{2}$$

where ρ is the density, t time, \vec{V} velocity, $\bar{\tau}$ stress, p pressure and \vec{F} the body force. The turbulence feature of fluid flow is taken into account by using the Realizable $k-\varepsilon$ model [24]:

$$\frac{\partial(\rho k)}{\partial t} + \nabla \cdot (\rho k \vec{V}) = \nabla \cdot \left[\left(\mu + \frac{\mu_t}{\sigma_k} \right) \nabla k \right] + G_k - \rho \varepsilon, \quad (3)$$

$$\frac{\partial(\rho \varepsilon)}{\partial t} + \nabla \cdot (\rho \varepsilon \vec{V}) = \nabla \cdot \left[\left(\mu + \frac{\mu_t}{\sigma_\varepsilon} \right) \nabla \varepsilon \right] + C_1 \rho E \varepsilon - \rho C_2 \frac{\varepsilon^2}{k + \sqrt{\nu \varepsilon}}, \quad (4)$$

$$\mu_t = C_u \rho \frac{k^2}{\varepsilon}, \quad (5)$$

where k is the turbulence kinetic energy, ε the turbulent dissipation rate and μ_t the turbulent viscosity. The rest of the parameters are all in connection with the features of turbulence and can be found in [24]. In order to properly formulate the fluid flow near the rigid walls, the enhanced wall treatment [25] is employed here. It is valid to formulate the fluid flow features throughout the whole near-wall region (including the viscous sublayer, buffer region, and log-law region), across which the fluid flow can vary from fully laminar to fully turbulent. The interface between the liquid metal and air is implicitly captured by the volume of fluid (VOF) method [26]:

$$\frac{\partial(\alpha_i)}{\partial t} + \nabla \cdot (\alpha_i \vec{V}_i) = 0, \quad (5)$$

where α is the volume fraction of the phase i in a control volume. By determining the volume fraction of all the phases ($i=1,2$ in the liquid-gas two phase system of this paper) in the control volumes using the transport equation of Eq.5, the scalar properties of control volumes that resolve the liquid-gas interface can be determined by using appropriate method of averaging (e.g. mass weighted average with regard to density). Therefore, only a single momentum equation (Eq.2) and a single continuity equation (Eq.1) have to be solved, which makes this method of two-phase fluid flow simulation computationally economical. In the computational results, all the variables (such as pressure and velocity etc.) are shared by all the phases. When calculating the flux of parameters of interest at the walls of the control volumes that represent the liquid-gas interface, the geometric reconstruction method [27] is

1 used, which reconstructs the interface between fluids using a piecewise-linear approach based
2 on the value and derivatives of the volume fraction α .

3
4 In the computation, the surface of the rotor, stator and static DC caster are all assumed to be
5 rigid walls, at which the non-slip boundary condition of the fluids is assumed. The surface
6 tension at the liquid-air interface is formulated by using the continuum surface force model
7 [28], which maps the surface force onto the control volumes that are near the liquid-air
8 interface.
9

10
11 The rotor spins at high speed and it strongly agitates the fluid. The sliding mesh method [29]
12 is employed in order to take the rotational movement of the impeller and its influence on the
13 fluid flow into account. When applying the sliding mesh method, the mesh of fluid(s) zone is
14 partitioned into multiple subzones, which share non-conformal interfaces. As the rigid walls
15 of the rotor move, the corresponding subzones of the fluid (e.g. the fluid subzone that closely
16 surrounds the rotor) correspondingly move in a rigid way (i.e. there is no deformation of the
17 mesh). This method is believed to be a better method for formulating the model of fluid
18 agitation by the close coupled rotor-stator mixer than the alternative method that moves the
19 reference frame.
20
21

22
23 The overall simulation domain is discretized with tetrahedral mesh of adaptive resolution, in
24 order to resolve the geometrical features of different sizes at different places of the domain.
25 The mesh size varies between around 0.1 mm and 5 mm. The overall governing equations are
26 solved with the SIMPLE method [30], in order to find the transient solution of the target
27 problem. The size of the time step is 5×10^{-4} s. The computation was implemented by using the
28 FLUENT module of ANSYS, and the details of the related mathematical models and
29 computation can be found in [29]. In the computation, the value of density and dynamic
30 viscosity of the liquid aluminium alloy and the surface tension coefficient of the melt-air
31 interface was employed as 2700 kg/m^3 [31], $0.0027 \text{ Pa}\cdot\text{s}$ [32] and 0.87 N/s [33] respectively.
32
33
34
35
36
37
38
39
40
41
42
43
44
45
46
47
48
49
50
51
52
53

54 3. Simulation results

55 3.1 Net mass flow rate through the mixing head

56
57
58
59
60
61
62
63
64
65

We firstly analyzed the temporal evolution of the mass flow rate of the liquid metal through the stator holes; Fig. 2. As can be seen from Fig.1, there are four rows of holes at the side of the stator. The mass flow rates through the various rows are different. The mass flow rate through the first row of holes, near the bottom of the mixing head, is relatively low in magnitude and has a negative sign. This means that the liquid metal is actually flowing into the mixing head through this row of holes. The rate of melt flow through the second and fourth rows of holes is comparatively higher, and flowing out of the mixing head. The flow rate through the third row of holes of the stator is the greatest. Summing the mass flow rate through all four rows of stator holes, we find the net mass flow rate of the liquid metal flowing out of the mixing head. In Fig.3, we see that the total net mass flow rate through the mixing head reaches a plateau value of 0.12 kg/s after 0.71 s of shearing. In the following part of this section, we analyze related flow features of the liquid metal at this moment of 0.71 s of shearing.

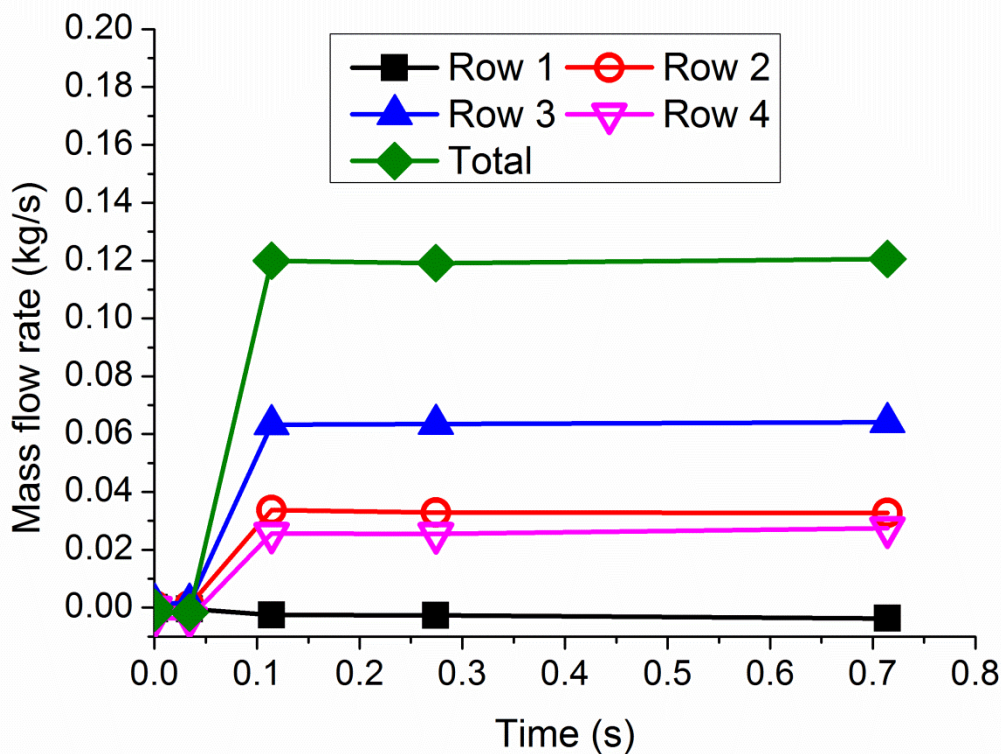


Fig.3. Temporal evolution of the mass flow rate of the liquid metal flowing through the mixing head

3.2 Flow pattern inside the mixing head

1
2
3
4
5
6
7
8
9
10
11
12
13
14
15
16
17
18
19
20
21
22
23
24
25
26
27
28
29
30
31
32
33
34
35
36
37
38
39
40
41
42
43
44
45
46
47
48
49
50
51
52
53
54
55
56
57
58
59
60
61
62
63
64
65

In order to analyze the flow pattern inside the mixing head, we sample the velocity of liquid metal along a virtual interface of revolution in parallel to the shaft of the impeller of 16 mm in diameter, as shown by the vectors in Fig.4. It can be seen that the liquid metal flows upwards into the mixing head from its bottom near the root of the impeller blades. This upward flowing stream of liquid metal quickly changes its direction from axial to circumferential. While sampling the velocity of fluid flow along a central plane through the rotor shaft which bisects two facing columns of holes, as shown in Fig.5, it can be seen that there is a very weak recirculation of the liquid metal inside the mixing head along its length which is accompanied by the outward flow of the liquid metal through the holes of the stator at its side.

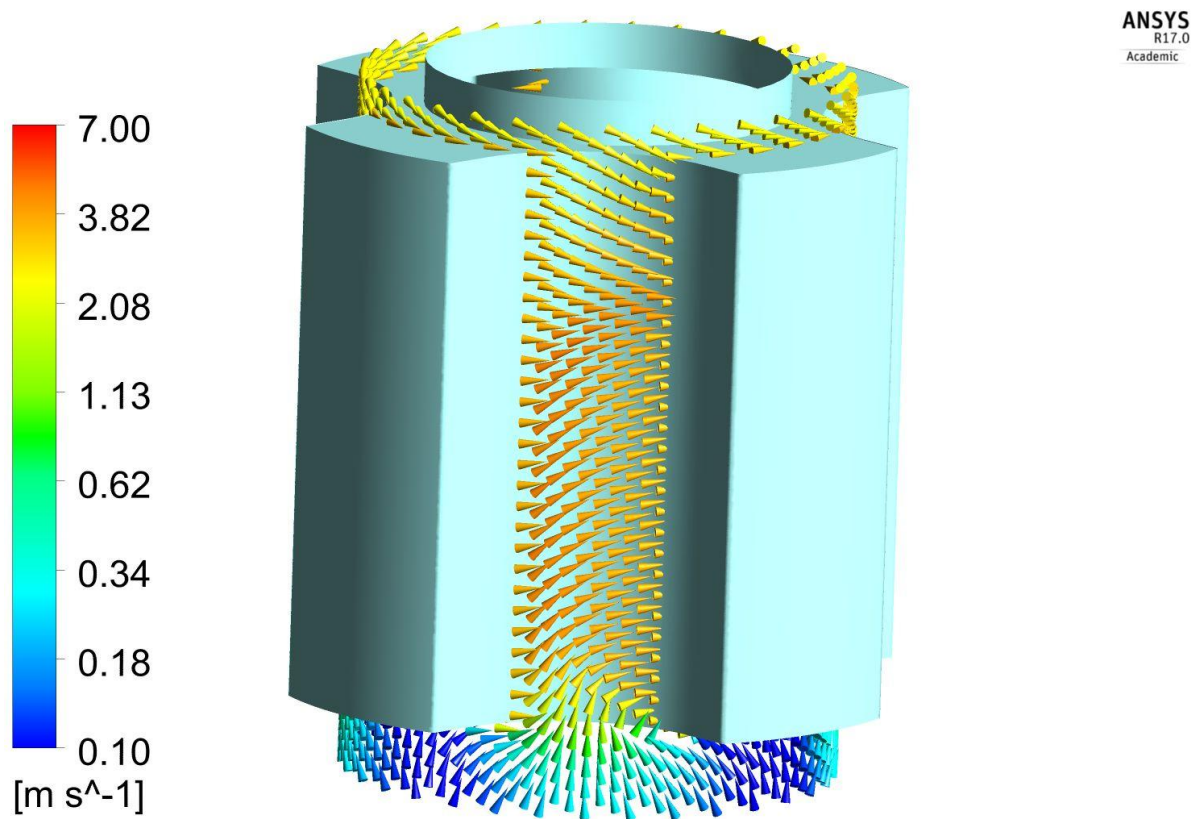


Fig.4. Velocity vectors of the liquid metal along a surface of revolution of 16 mm in diameter, parallel to the shaft of the impeller, at 0.71 s.

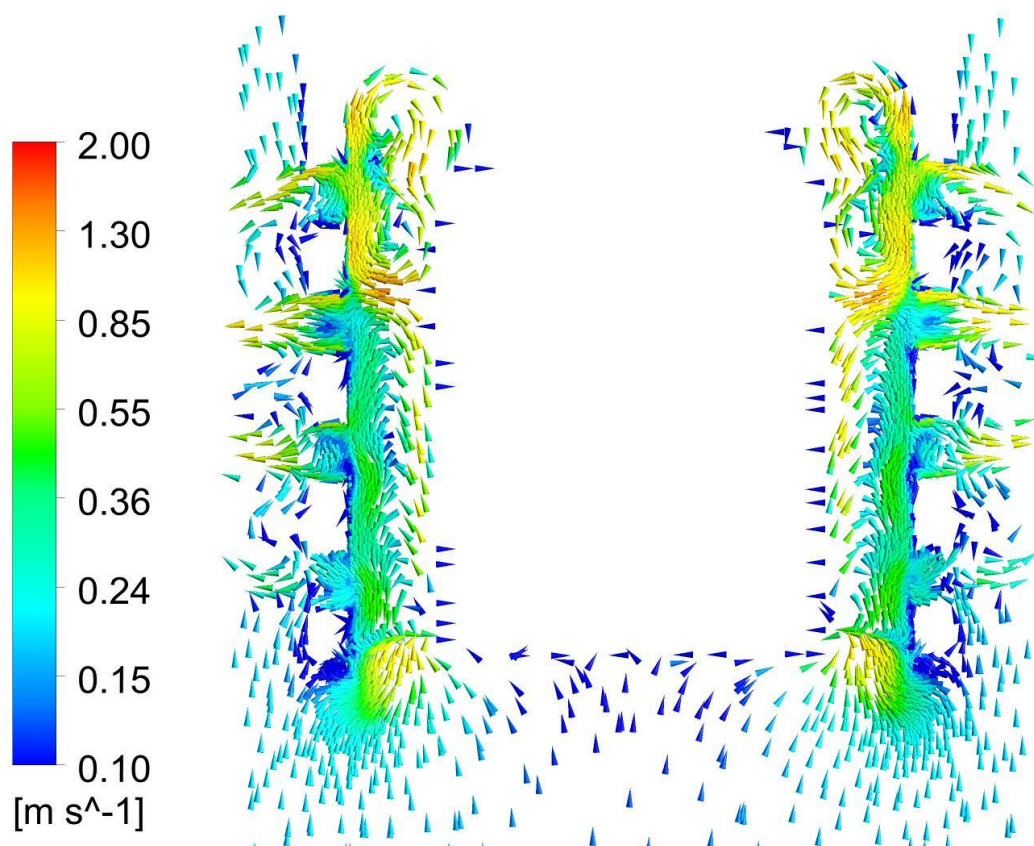


Fig.5. Velocity vectors of the liquid metal projected to a plane that is along the center of the rotor shaft around the mixing head, at time 0.71 s of shearing

The pressure field inside the mixing head, as shown in Fig.6, caused such a melt flow pattern inside the mixing head. Due to interactions between the flowing liquid metal, the moving impeller and the stationary stator, a high pressure zone occurs near the internal surface of the mixing head around the third row of holes. This high pressure zone creates an outward pressure gradient, which drives the liquid metal out of the mixing head. At the same time, due to the centrifugal force, a low pressure zone occurs near the root of the impeller blades around the bottom of the mixing head. This low pressure zone sucks the liquid metal into the mixing head from below. Near the large opening at the bottom of the mixing head, the low pressure zone extensively expands from the root of impeller blades towards the internal orifice of the first row of holes of the stator at its side. Therefore, the liquid metal is actually flowing into the mixing at a very low rate through the holes of the first row, instead of flowing out.

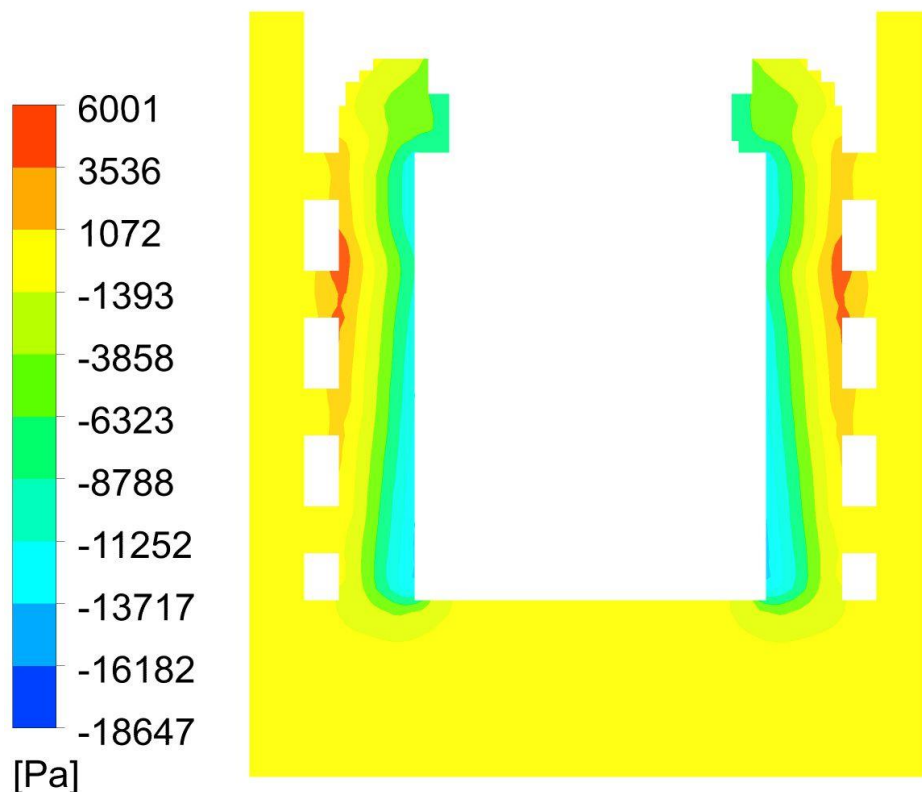
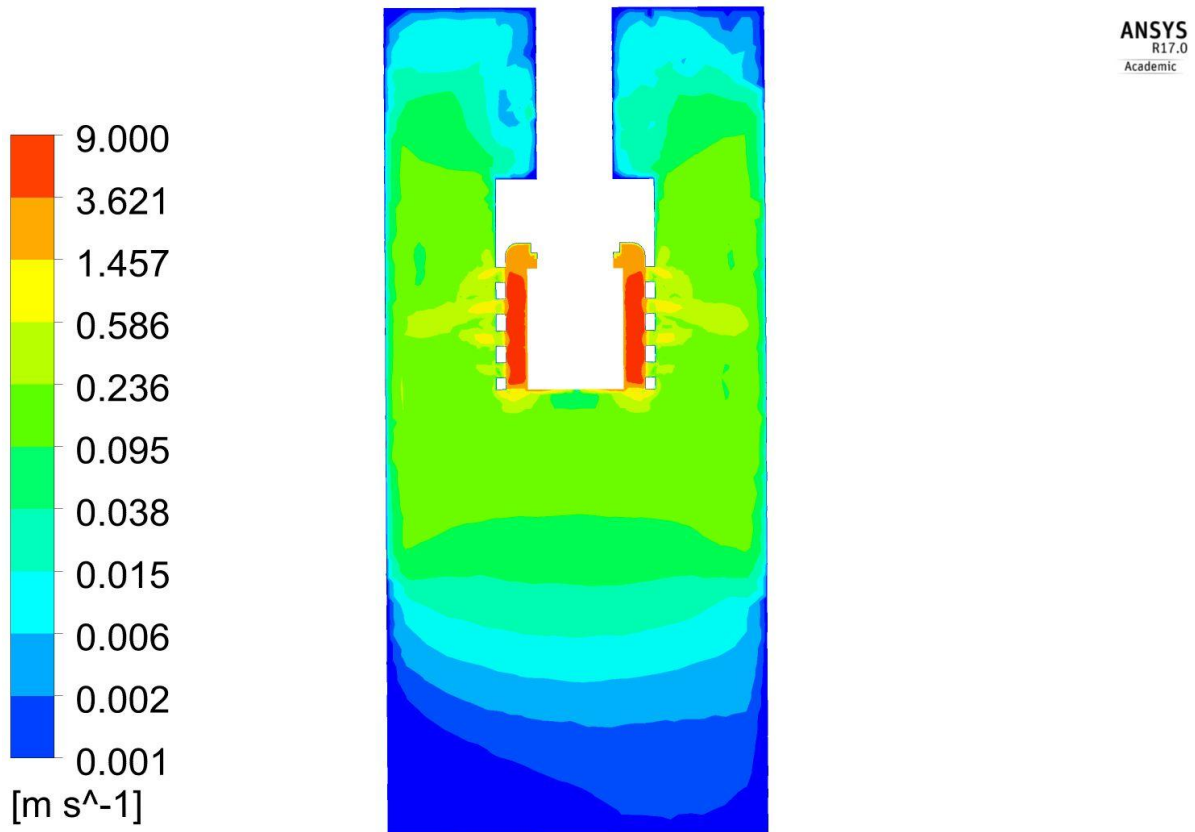


Fig.6. Contour of pressure at a plane that is along the centre of the shaft rotor, at 0.71 s.

3.3. Fluid agitation in the overall caster

In order to characterise how well the bulk liquid metal is agitated, we zoom out to the scale of the overall caster. Figure 7 illustrates the melt flow field in a central plane that is along the shaft of the rotor. The model predicted that, while the liquid melt is flowing at a very high speed inside the mixing head, it is very quickly and dramatically decelerated as soon as it shoots out of the mixing head through the stator holes. Because the circumferential and axial profile of the magnitude of the melt velocity is highly non-uniform, we sampled the maximum melt velocity along virtual surfaces of revolution, 20 mm high (starting from the bottom of the mixing head upwards), and of different diameters, near the mixing head and parallel to the shaft of the rotor, and used it as the representative velocity of the melt jets that shoot out of the mixing head. As shown in Fig.8, the velocity of melt jets evolves from around 5.1 m/s down to around 1.2 m/s while shooting out of the mixing head. Within a distance of 10 mm outside the stator (between the radial position of 15 mm and 25 mm

1
2 relative to the shaft), the melt velocity decreases from 1.2 m/s to 0.4 m/s. Such dramatic
3 deceleration is due to the fact that the momentum of the outshooting liquid metal jets is
4 comparatively low, since the diameter of the holes at the side of the stator is very small
5 compared with the diameter and depth of the overall caster. Therefore, the velocity of the
6 melt jets is very quickly dissipated by the comparatively stagnant bulk liquid metal of the
7 overall caster, due to conservation of momentum. The comparatively high viscosity of liquid
8 metal also contributes to the damping of the velocity of the outshooting liquid metal jets.
9
10
11
12



41
42
43 Fig.7. Contour of the magnitude of the velocity of liquid metal at a central plane, at 0.71 s.
44
45
46
47
48
49
50
51
52
53
54
55
56
57
58
59
60
61
62
63
64
65

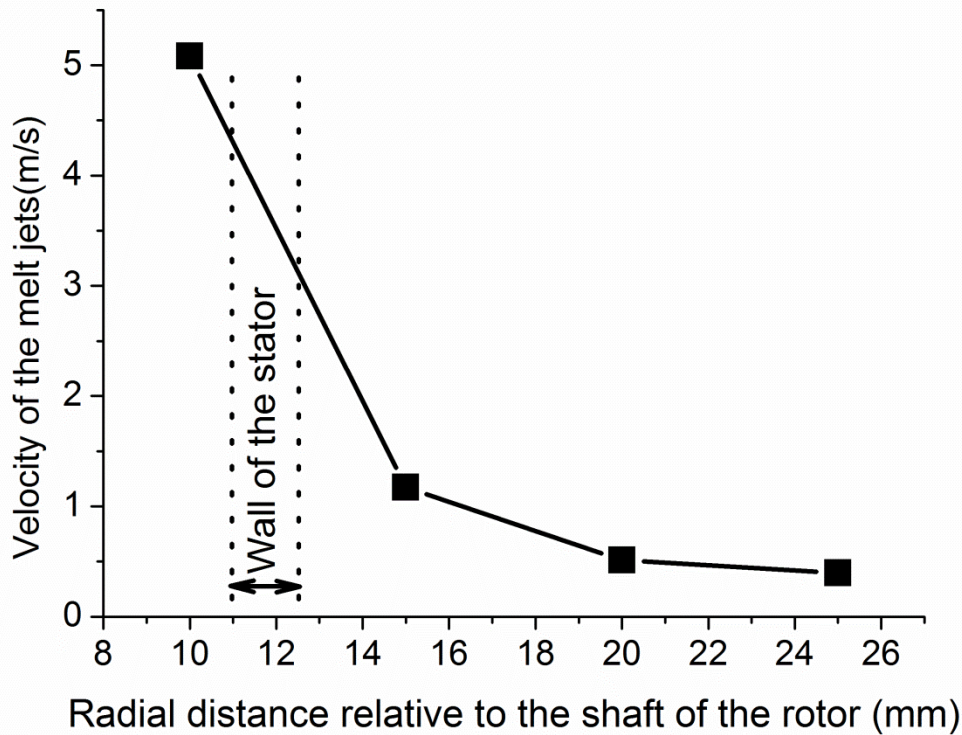


Fig.8. Radial profile of the maximum magnitude of the melt velocity in the close vicinity of the mixing head, at 0.71 s.

Analysis of the stream lines of fluid flow, as shown in Fig.9, shows how the liquid metal is redistributed throughout the overall caster. In the close vicinity of the mixing head, there are two strong counter-rotating recirculations of the liquid metal above and below the third row of stator holes. The melt recirculation above the third row of holes is so localized and strong that the bulk liquid metal above the third row of the holes of the stator has very little chance to flow into the mixing head. The melt recirculation below row 3 entrains some bulk liquid metal into the mixing head, mainly through the large opening at the bottom of the mixing head, and is sheared. Below the mixing head, the melt flows at relatively low velocity, particularly near the bottom of the caster. Comparing Fig.9 with Fig.8, we conclude that only the melt in the close vicinity of the mixing head is well agitated by the mixer, and only that part below the third row of stator holes has a good chance to be redistributed via the mixing head.

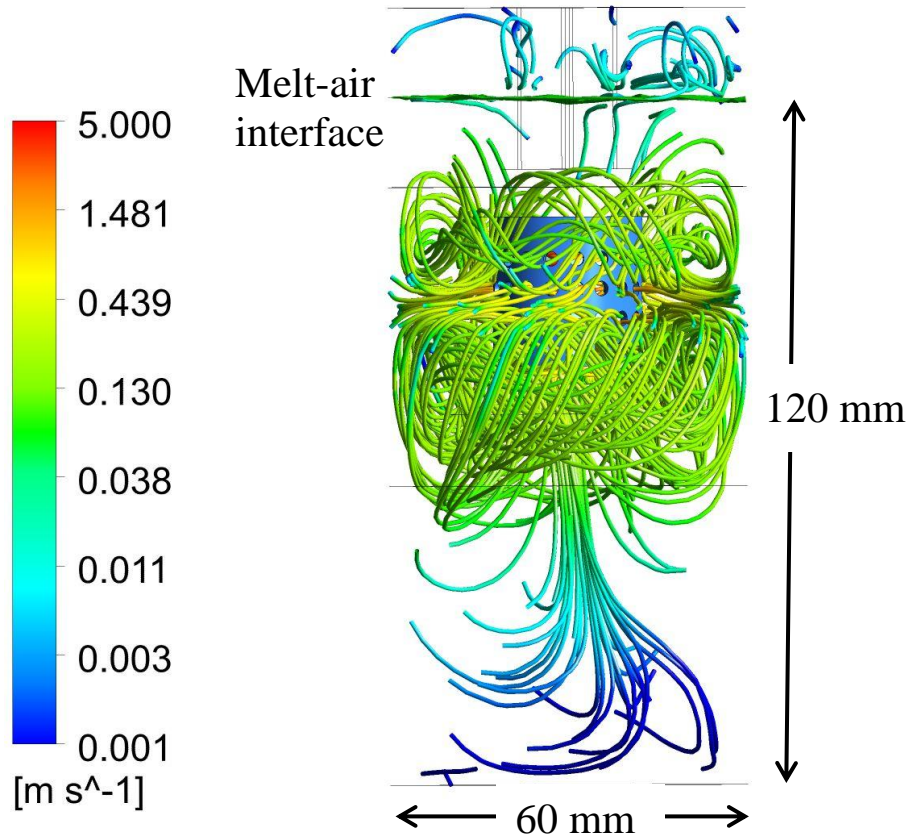


Fig.9. Stream lines of fluid flow, at the time of 0.71 s.

3.4. Shear rate

Shear is a very important phenomenon in HSP. The liquid shear rate is responsible for the dynamics of agglomeration and breakage of the dispersed phases. Before calculating the value of shear rate, we have to firstly determine if the fluid flow is laminar or turbulent. When the fluid flow is laminar, the shear rate is the gradient of the velocity of fluid (assuming the fluid is incompressible). When the fluid flow is turbulent, shear rate is a function of the turbulence dissipation rate as:

$$\sigma = \sqrt{\frac{\varepsilon}{\nu}}, \quad (6)$$

where σ is the characteristic shear rate, ε is the turbulence dissipation rate, and ν is the kinematic viscosity of the melt. As shown in Fig.10, in the overall caster, the value of viscosity ratio (ratio of the turbulent viscosity to the physical viscosity) is mostly above 20. This means that the fluid flow in the whole caster falls in the regime of turbulent flow.

Therefore, we use the turbulence dissipation rate and Eq.6 when computing the shear rate of the melt.

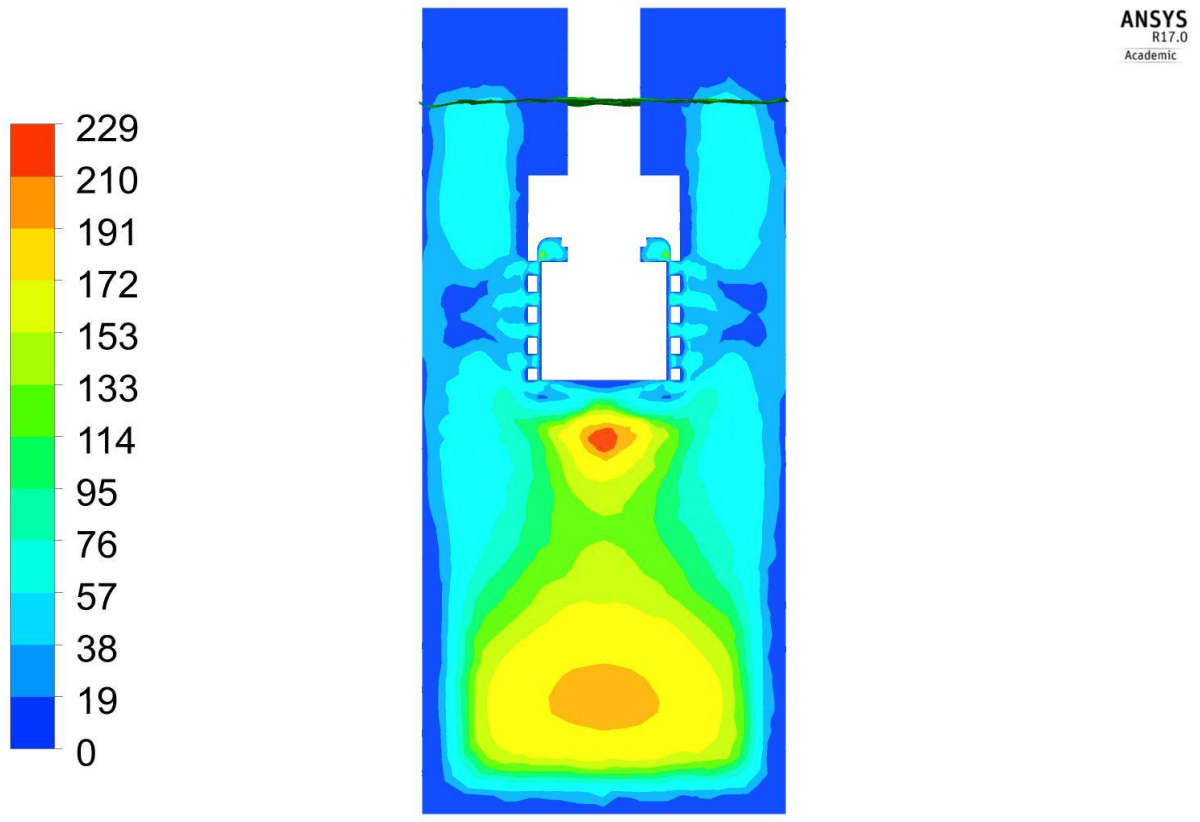


Fig.10. Contours of turbulent viscosity ratio at a central plane through the shaft of the rotor, at 0.71 s.

The contours of turbulence dissipation rate that are shown in Fig.11 illustrate that values of turbulence dissipation rate are relatively high in the close vicinity of the mixing head (and particularly between the rotor and the stator) and the value in the far field of the bulk melt is relatively low. This means that we can only expect high level of shear rate in the close vicinity of the mixing head.

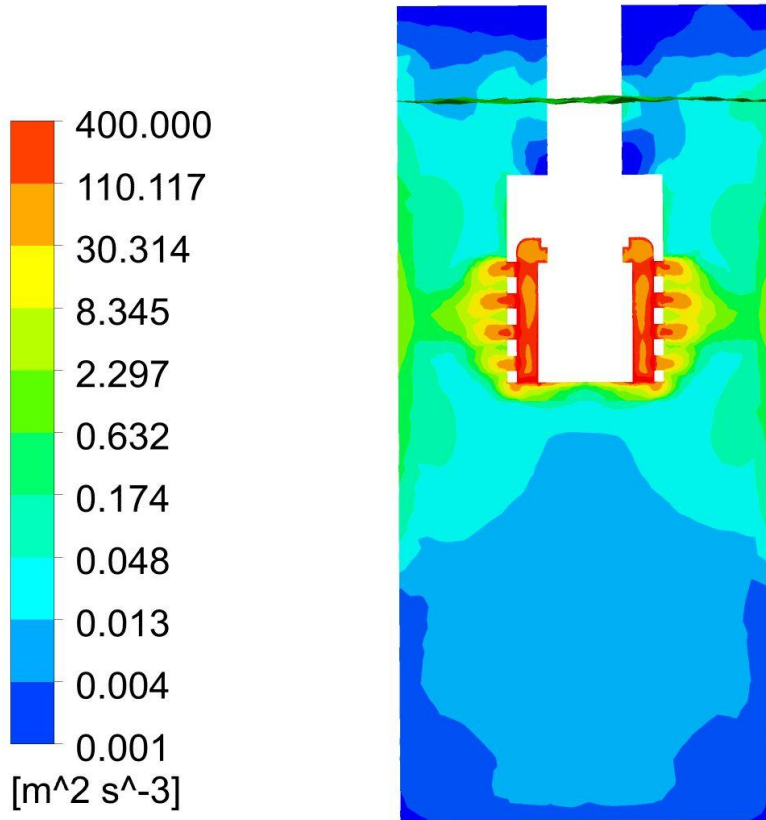


Fig.11. Contours of turbulence dissipation rate at a central plane along the shaft of the rotor, at 0.71 s.

If we sample the value of turbulence dissipation rate on a plane that is normal to the shaft of rotor along the third row of stator holes, as shown in Fig.12, we can clearly see its radial and circumferential profile. Inside the mixing head (particularly inside the gap between the rotor and the stator and inside the stator holes), the level of the turbulence dissipation rate is relatively high. Outside the mixing head however, the level is quite low. Along the circumference of the mixing head, the circumferential profile of the turbulence dissipation rate follows the geometrical features of the stator (i.e. size and spacing of the holes in its wall) and the rotor (i.e. size and number of blades).

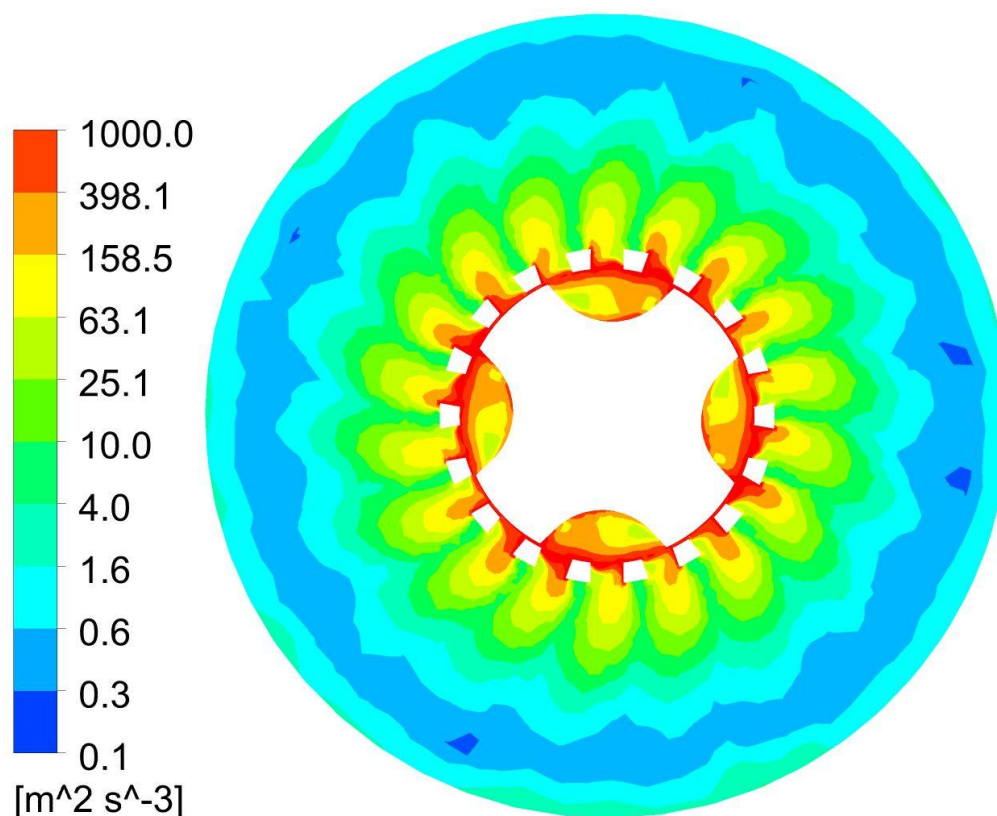


Fig.12. Contour of the turbulence dissipation rate at a plane normal to the shaft of the rotor, at row 3 of stator holes, at 0.71 s.

Quantitatively, we computed the maximum value of the characteristic shear rate at different virtual surfaces of revolution, again 20 mm high (starting from the bottom of the mixing head upwards), and of different diameters, parallel to the shaft of the rotor around the mixing head, and used it as the representative shear rate as a function of the radial position of the melt as shown in Fig.13. We can see that the shear rate has the highest value of $1.11 \times 10^5 \text{ s}^{-1}$ inside the mixing head (radial position of 10 mm). The value of the shear rate decreases by around an order of magnitude (down to $1.14 \times 10^4 \text{ s}^{-1}$) as the melt flows out of the holes of the stator (i.e up to radial position of 15 mm). As the melt flows near the wall of the caster (radial position of 25 mm), the value of shear rate further decreases by another order of magnitude (down to 960 s^{-1}). The results shown in Fig.13 show that, due to the closed coupled feature of the rotor-stator mixer, there is a high level of shear rate only inside the mixing head; elsewhere the shear rate is relatively low.

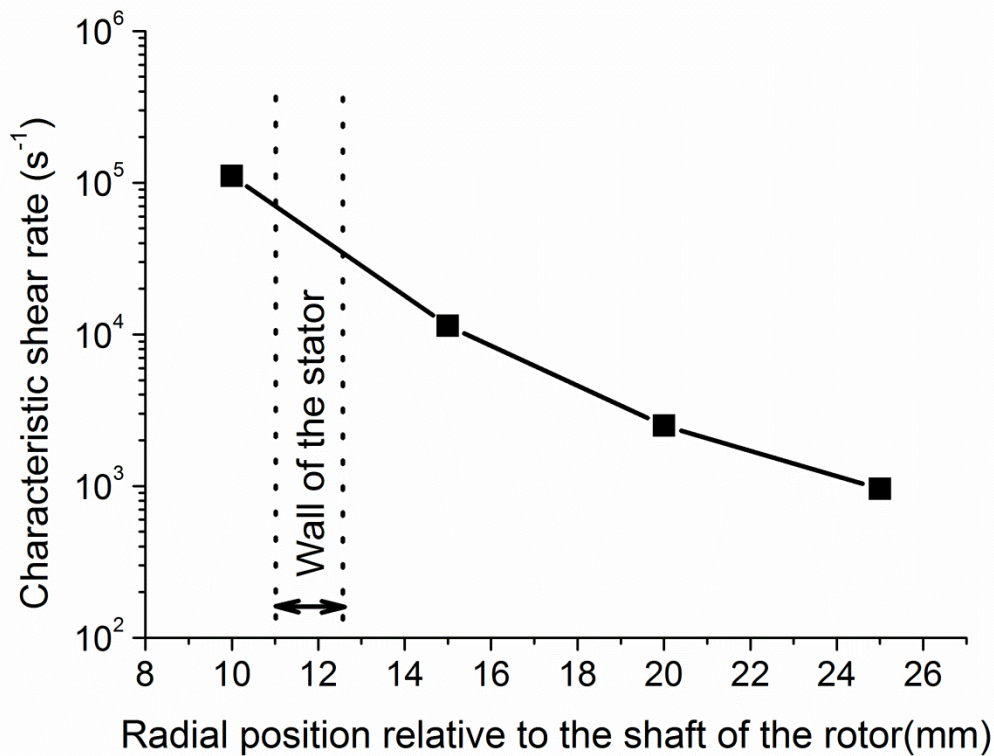


Fig.13. Radial profile of the maximum characteristic shear rate at 0.71 s.

3.5 Experimental validation

In the experimental research of Jones et.al. [23], HSP was employed in the treatment of molten AA6060 alloy in a static DC caster. The process parameters that were employed in the presented computer simulation were chosen to agree well with those that were used in the previous experiments [23] on commercially pure aluminium (alloy AA 60060). So the modelling results are directly relevant to those experimental findings.

The microstructure of the solidified alloy billet was characterised with optical metallography, and dramatic variation of the microstructure was found along the height of the billet. As shown in Fig.14, near the bottom of the billet, the dendrites are coarse columnar dendrites parallel to the billet axis, which is followed by a second zone of columnar dendrites that tilt at an angle to the lower ones. Above the second zone of columnar dendrite, there is a zone of very refined equiaxed dendrites. Above the fine equiaxed dendrite zone, there is a second

1 zone of coarser equiaxed dendrites. Jones et.al. [23] deduced qualitatively that it was the
2 influence of melt flow features that caused such variation of microstructure along the height
3 of the solidified billet, due to oxide fragmentation caused by melt shear. These oxides act as
4 nucleating agents for Fe-based intermetallics and then primary aluminium. They placed the
5 mixing device at a similar depth as that used in our simulations, switched it on and removed it
6 from the crucible whilst the melt was still superheated.
7
8
9
10
11
12
13
14
15
16
17
18
19
20
21
22
23
24
25
26
27
28
29
30
31
32
33
34
35
36
37
38
39
40
41
42
43
44
45
46
47
48
49
50
51
52
53
54
55
56
57
58
59
60
61
62
63
64
65

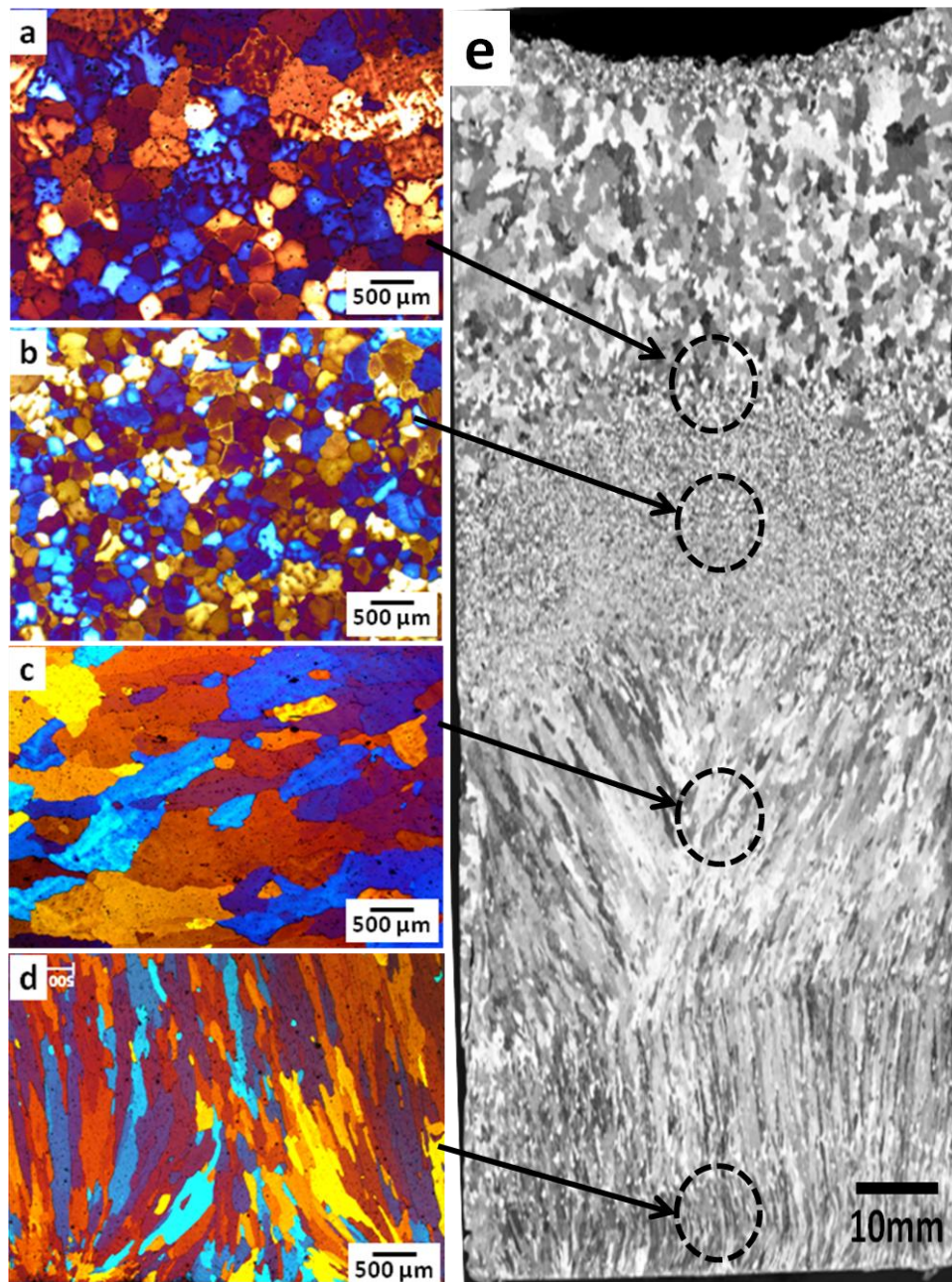


Fig.14. Microstructure of the solidified AA6060 billet (reproduction of Fig.5 of [23]).

1 In order to quantitatively analyze the possible influence of melt flow features on the
2 microstructure of the solidified billet via our computational model, when analysing the
3 simulation results, we section the height of the melt with several virtual planes that are
4 normal to the height of the caster. The maximum value of the characteristic shear rate and the
5 area-averaged absolute value of the component of the melt velocity that is normal to these
6 virtual planes are sampled. In the meanwhile the grain size was experimentally measured at
7 the representative positions shown in Fig. 14 (a-d). The variation of the maximum shear rate,
8 average absolute velocity of the melt along the depth, and grain size of the solidified billet are
9 illustrated in Fig.15 as a function of height relative to the bottom of the caster.
10
11
12
13
14
15
16
17
18
19
20
21
22
23
24
25
26
27
28
29
30
31
32
33
34
35
36
37
38
39
40
41
42
43
44
45
46
47
48
49
50
51
52
53
54
55
56
57
58
59
60
61
62
63
64
65

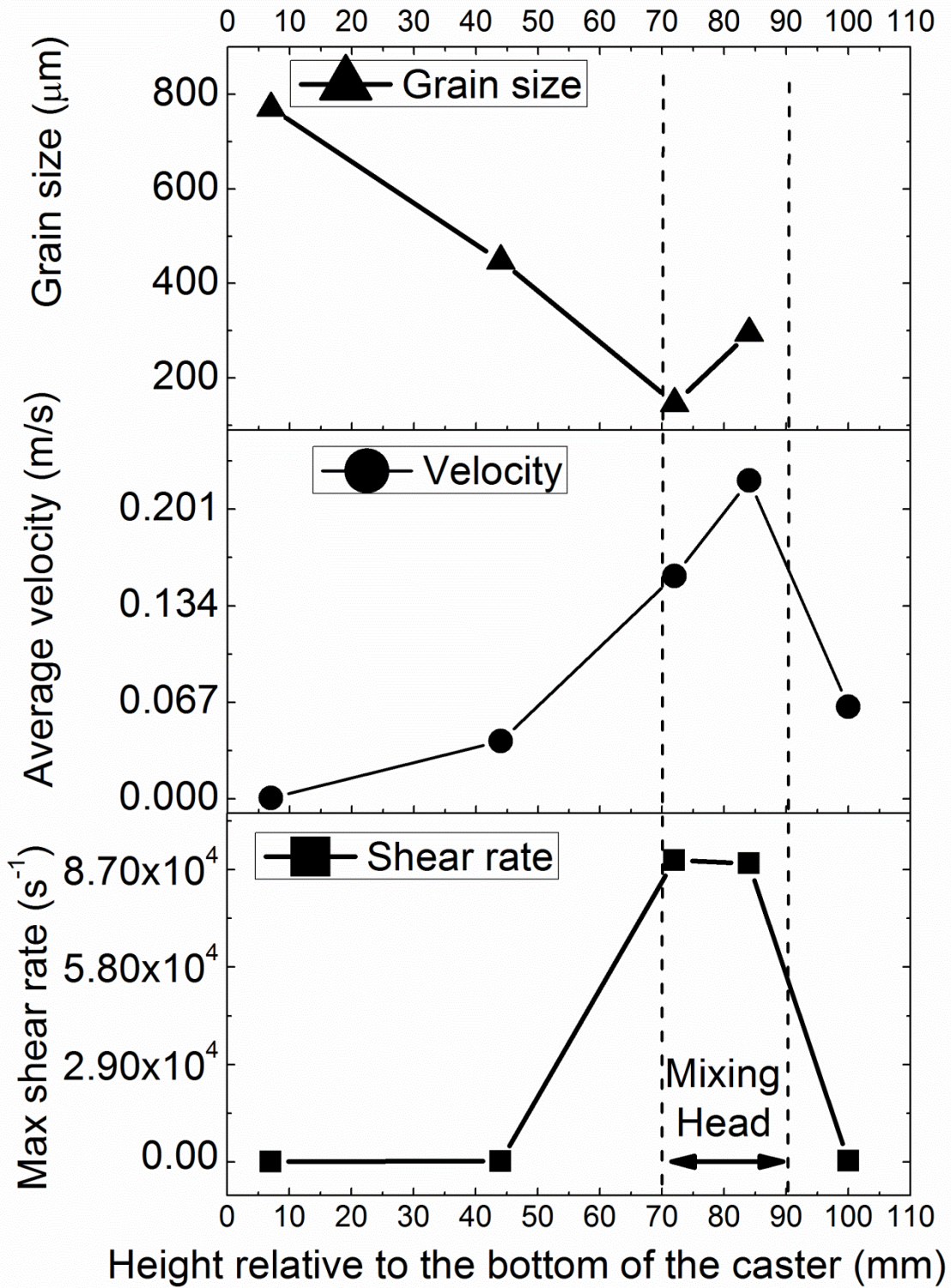


Fig.15. Variation of grain size, area averaged vertical component of melt velocity, and maximum characteristic shear rate, and through the height of the caster.

1 We can find a clear link between the variation of these three different parameters along the
2 height. In the close vicinity of the mixing head, between a height of 70 mm and 90 mm, there
3 is a very high level of shear rate and vertical component of melt velocity. Because the vertical
4 component of melt velocity characterises the efficiency of the redistribution of the liquid
5 metal from the depth of the caster into the mixing head, this result means that the liquid metal
6 in this range of the depth of the caster is very quickly redistributed through the mixing head
7 where it is dramatically sheared. The resultant vast fine and uniformly distributed oxide
8 particles can act as potent nuclei that dramatically improve the nucleation of equiaxed
9 dendrites inside this region. The dramatic event of nucleation of equiaxed dendrite can trigger
10 the columnar to equiaxed transition (CET) [34], which leads to the small size equiaxed
11 dendrites as shown in Fig.14 (a,b) and Fig.15. Below the fine equiaxed dendrite zone, as
12 shown in Fig.14 and 15, the level of shear rate and vertical component of melt velocity are
13 relatively low. Particularly, the level of shear rate is negligible. This means that the liquid
14 metal is not effectively sheared in this region, and it has very little chance to be redistributed
15 into the mixing head and get sheared either. Therefore there are not enough fine and
16 uniformly distributed oxide particles which can result in significant nucleation of equiaxed
17 dendrites, in this region. The columnar growth of dendrites in this region is dominant, due to
18 the chilling effect by the bottom of the caster. Above the zone of fine equiaxed dendrite, there
19 is a second zone of coarse equiaxed dendrite. Firstly, the sequence of solidification of the
20 billet is from the bottom towards the top. Because CET already occurs in the zone of fine
21 equiaxed dendrites, the solidification has to proceed in the form of equiaxed dendrite from
22 here upwards. Secondly, in this second zone of coarse equiaxed dendrites, the level of shear
23 rate and vertical component of melt velocity is relatively low. The melt is not effectively
24 sheared in this zone and it has very little chance to be redistributed into the mixing head and
25 get effectively sheared either, which can be also found in the localized recirculation of melt
26 as shown in the stream line of Fig.9. Therefore there is a comparatively lower number of
27 oxide particles acting as effective nuclei in this region. This results in the coarse equiaxed
28 microstructure here.

4. Discussion and conclusion

51 By analysing key features of fluid flow during HSP of aluminium alloy, using computer
52 simulation, we found that the distribution of related parameters of the melt flow is highly
53 nonuniform in space. Overall, in the close vicinity of the mixing head, there is relatively high
54
55
56
57
58
59
60
61
62

1 level of shear rate. Particularly, inside the gap between the rotor and the stator, the level of
2 shear rate is very high, while the level in the far field of the bulk liquid metal is much lower –
3 by a few orders of magnitude. This means that only the melt that can flow through the mixing
4 head is well sheared. The liquid metal is well agitated only in the close vicinity of the mixing
5 head, while the melt deep in the caster is relatively stagnant. Particularly, the melt above the
6 third row of the holes of the stator is found to have little chance flowing into the mixing head.
7 This feature of fluid agitation means that only the melt that is in the close vicinity of the
8 mixing head and below the third row of the holes will be well sheared by the mixer. This
9 conclusion is positively supported, but not directly validated, by the microstructure of the
10 solidified billet of the HSP treated molten alloy.
11
12
13
14
15
16
17
18
19

20 For full model validation we will have to include computational treatment of heat transfer
21 during the process, grain nucleation and CET formation [34], in order to link nucleation
22 density and potency [35] to grain structure and grain size. This is beyond the scope of the
23 current contribution. However we have already shown in a separate contribution [12] that
24 there is a direct link between shear rate and oxide fragmentation in HSP. So, in theory, a high
25 shear rate should lead to CET and formation of small equiaxed grains, as has been shown to
26 be the case in Fig. 15. We have not validated the current model yet, but rather we have
27 highlighted confidence-building experimental evidence.
28
29
30
31
32
33
34
35

36 The computationally predicted features of the HSP of liquid metal with the rotor-stator mixer
37 has a two-fold influence on its application. The positive aspect is that the performance of the
38 mixer is not affected by the geometry (i.e. shape, volume, and relative position) of the
39 container that holds the liquid metal. It makes the design and optimisation of the rotor-stator
40 mixer independent of the environment in which it is going to be applied. For example, the
41 level of shear rate and level of mass flow rate in the close vicinity of the mixing head do not
42 significantly vary when treating either 50 kg or 200 kg of liquid metal. Therefore, the
43 optimised rotor-stator is universal to the varying contexts of application to some extent.
44 However, a negative aspect is that is difficult to shear the liquid metal in the far field of the
45 container effectively. Although the shear rate and mass flow rate in the close vicinity of the
46 mixing head are not affected by changes in container size or shape, when treating a large
47 volume of liquid metal with this rotor-stator mixer a significant part of the bulk liquid not
48 effectively sheared. Due to the specific geometrical feature of the rotor-stator mixer, the inlet
49 for liquid (i.e. the large opening at the bottom of the mixing head) and the outlet (i.e. the
50
51
52
53
54
55
56
57
58
59
60
61
62
63
64
65

1
2
3
4
5
6
7
8
9
10
11
12
13
14
15
16
17
18
19
20
21
22
23
24
25
26
27
28
29
30
31
32
33
34
35
36
37
38
39
40
41
42
43
44
45
46
47
48
49
50
51
52
53
54
55
56
57
58
59
60
61
62
63
64
65

holes at the side of the stator) are very close to one another. This fact results directly in the highly localized strong recirculation of liquid as shown in Fig.9, which is the key reason for the difficulty of agitating the melt deep in the caster.

Overall, HSP of liquid metal with the rotor-stator mixer can shear the liquid metal very well in the close vicinity of the mixing head. If it can be improved in order to effectively agitate a larger volume of liquid metal, it has great potential of application in the industrial scale treatment of molten alloys, for the purpose of purification.

Acknowledgement

This work is financially supported by the European Commission FP7 project “High shear processing of recycled aluminium scrap for manufacturing high performance aluminium alloys”; Grant Number 603577.

References

1. S. Jones, A. K. Prasada Rao, Z. Fan, Melt conditioned direct chill (MC-DC) casting of Al alloys, *Trans Indian Inst Met.* 66 (2013) 117–121
2. M. Xiaa, A.K. Prasada Raob and Z. Fan, Solidification mechanisms in melt conditioned direct chill (MC-DC) cast AZ31 billets, *Materials Science Forum.* 765 (2013) 291-295
3. Y. B. Zuo, B. Jiang, Y. Zhang, Z. Fan, Grain refinement of DC cast magnesium alloys with intensive melt shearing, *IOP Conf. Series: Materials Science and Engineering* 27 (2011) 012043
4. G. Scamans, H. Li and Z. Fan, Melt conditioned casting of aluminium alloys, 13th International Conference on Aluminum Alloys (ICAA13), 2012, 1395-1400
5. H. T. Li, Y. Wang and Z. Fan, Enhanced heterogeneous nucleation on oxides in Al alloys by intensive shearing, *IOP Conf. Series: Materials Science and Engineering.* 27 (2011) 012047
6. S. Ji, W. Yang, F. Gao, D. Watson, Z. Fan, Effect of iron on the microstructure and mechanical property of Al–Mg–Si–Mn and Al–Mg–Si die cast alloys, *Materials Science & Engineering A.* 564 (2013) 130–139
7. H. T. Li, S. Ji, Y. Wang, M. Xia and Z. Fan, Effect of intensive melt shearing on the formation of Fe containing intermetallics in LM24 Al-alloy, *IOP Conf. Series: Materials Science and Engineering.* 27 (2011) 012075
8. W. Yang, S. Ji, X. Zhou, I. Stone, G. Scamans, G. E. Thompson, and Z. Fan, Heterogeneous nucleation of α -Al grain on primary α -AlFeMnSi intermetallic investigated using 3D SEM Ultramicrotomy and HRTEM, *Metallurgical and Materials transactions A.* 45 (2014) 3971
9. Z. Fan, Y. Wang, Z. F. Zhang, M. Xia, H. T. Li, J. Xu, L. Granasy and G. M Scamans, Shear enhanced heterogeneous nucleation in some Mg- and Al-alloys, *International Journal of Cast Metals Research.* 22 (2009) pp 1-5
10. R. Haghayegi, L. Nastac, On microstructural refinement of an AA7449 aluminium alloy through shearing above liquidus temperature, *Materials Letters.* 65 (2011) 3230-3233
11. X. Fang, G. Shao, Y.Q. Liu, Z. Fan, Effects of intensive forced melt convection on the mechanical properties of Fe-containing Al-Si based alloys, *Materials Science and Engineering A.* 445–446 (2007) 65–72

12. M. Tong, S. Jagarlapudi, J. Patel, I. Stone, Z. Fan, David J. Browne, Computational prediction of the refinement of oxide agglomerates in a physical conditioning process for molten aluminium alloy, IOP Conference Series: Materials Science and Engineering. 84 (2015), 012092.
13. X. Dong, X. Huang, L. Liu, L. He, P. Li, A liquid aluminium alloy electromagnetic transport process for high pressure die casting, Journal of Materials Processing Technology. 234 (2016) 217–227
14. L. Wu, J. Cheon, D. V. Kiran, S. Na, CFD simulations of GMA welding of horizontal fillet joints based on coordinate rotation of arc models, Journal of Materials Processing Technology. 231 (2016) 221–238
15. A. Kidess, M. Tong, G. Duggan, D.J., Browne, S. Kenjeres, I. Richardson, C.R. Kleijn, An integrated model for the post-solidification shape and grain morphology of fusion welds, International Journal of Heat and Mass Transfer. 85 (2015) 667-678
16. Y. Kwon, J. Zhang and H. Lee, A CFD-based nucleation-growth-removal model for inclusion behaviour in a gas-agitated ladle during molten steel deoxidation, ISIJ International, 48 (2008) 891–900
17. V. D. Felice, I. L. A. Daoud, B. Dussoubs, A. Jardy and J. Bellot, Numerical modelling of inclusion behaviour in a gas-stirred ladle, ISIJ International, 52 (2012) 1273–1280
18. P. Gardin, J.F. Domgin, M. Simonnet, J. Lehmann, Modeling of inclusion evolution in a steel ladle or in RH degasser, Revue de Metallurgie, 105 (2008) 84-91
19. J. Cheng, C. Yang, Z. Mao, and C. Zhao, CFD modelling of nucleation, growth, aggregation, and breakage in continuous precipitation of barium sulfate in a stirred tank, Ind. Eng. Chem. Res. 48 (2009) 6992–7003
20. Z. Fan, B. Jiang, Y. Zuo, Apparatus and method for liquid metals treatment, Patent US20130228045, 2013
21. A. T. Utomoa, M. Bakerb, A. W. Pacek, Flow pattern, periodicity and energy dissipation in a batch rotor–stator mixer, Chemical Engineering Research and Design. 86 (2008) 1397–1409
22. A. Utomoa, M. Bakerb, A.W. Pacek, The effect of stator geometry on the flow pattern and energy dissipation rate in a rotor–stator mixer, Chemical Engineering Research and Design. 87 (2009) 533–542

- 1
2
3
4
5
6
7
8
9
10
11
12
13
14
15
16
17
18
19
20
21
22
23
24
25
26
27
28
29
30
31
32
33
34
35
36
37
38
39
40
41
42
43
44
45
46
47
48
49
50
51
52
53
54
55
56
57
58
59
60
61
62
63
64
65
23. S. Jones, A. K. Prasada Rao, J. B. Patel, G. M. Scamans and Z. Fan, Microstructural evolution in intensive melt sheared direct chill cast al-alloys, in ICAA13: 13th International Conference on Aluminum Alloys (eds H. Weiland, A. D. Rollett and W. A. Cassada), John Wiley & Sons, Inc., Hoboken, NJ, USA, 2012, 91-96.
 24. T. H. Shih, W. W. Liou, A. Shabbir, Z. Yang, and J. Zhu, A new eddy-viscosity model for high reynolds number turbulent flows – model development and validation, *Computers Fluids*. 24 (1995) 227–238
 25. ANSYS® Academic Research, Release 17.0, Help System, "Turbulence", ANSYS, Inc.
 26. C.W. Hirt, B. D. Nichols, Volume of fluid (VOF) method for the dynamics of free boundaries, *Journal of Computational Physics*. 39 (1981) 201–225
 27. D. L. Youngs, Time-Dependent Multi-Material Flow with Large Fluid Distortion, *Numerical Methods for Fluid Dynamics*, K. W. Morton and M. J. Baines, editors, Academic Press. 1982.
 28. J. U. Brackbill, D. B. Kothe, and C. Zemach, A Continuum Method for Modeling Surface Tension, *J. Comput. Phys.* 100 (1992) 335–354.
 29. ANSYS® Academic Research, Release 16.2, Help System, Theory Guide, ANSYS, Inc.
 30. S. V. Patanker, D. B. Spalding, A calculation procedure for heat, mass and momentum transfer in three-dimensional parabolic flows, *International Journal of Heat and Mass Transfer*. 15 (1972) 1787-1806
 31. Y. Yitao, Z. Henghua and S. Guangjie, Application of computer simulation in developing automotive parts of Al alloy by using semi-solid die cast process, *Solid State Phenomena*. 116-117 (2006) 630-634
 32. Tables of Physical & Chemical Constants. 2.1.2 Barometry. Kaye & Laby Online. Version 1.1 (2008)
 33. J. Schmitz, J. Brillo, I. Egry, R. Schmid-Fetzer, Surface tension of liquid Al-Cu binary alloys, *Int. J Mat. Res.* 100 (2009) 1529-1535
 34. W.U.Mirihanage, H. J Dai, H.B.Dong, D.J. Browne, Computational modelling of columnar to equiaxed transition in alloy solidification, *Advanced Engineering Materials*. 15 (2013) 216-229
 35. A.G. Murphy, W.U. Mirihanage, D.J. Browne, R.H. Mathiesen, R.H., Equiaxed dendritic solidification and grain refiner potency characterised through in situ X-radiography, *Acta Materialia*. 95 (2015) 83-89